

Enhanced Optical Critical Dimension Metrology for the 7 nm Node and Beyond Using a Near-field Metalens

Jinlong Zhu ^{a,*}, Aditi Udupa ^a, Yating Shi ^b, Shiyuan Liu ^b, and Lynford L. Goddard ^{a,*}

*Email: lgoddard@illinois.edu; zhuwdwz1@illinois.edu PSL Group: <http://psl.mntl.illinois.edu/>

^a Photonic Systems Laboratory, Department of Electrical and Computer Engineering, University of Illinois at Urbana-Champaign, Urbana, USA

^b State Key Laboratory of Digital Manufacturing Equipment and Technology, Huazhong University of Science and Technology, Wuhan, China



INTRODUCTION

Optical scatterometry, which is a far-field based technique inherently, can be regarded as the most promising candidate technique to meet most of the rigid requirements of process control in the semiconductor industry^{1,2}. The critical dimension (CD) of the features of interest are presently below 20 nm and given current trends will likely reach the atomic scale in the mid-2020s. The downward scaling of the CDs and the increased structural complexity as well as the application of novel materials in semiconductor devices, brings up many grand challenges to the optical CD metrology, such as decreased sensitivity, varying optical properties of materials, tighter process specs, high correlations among fitting parameters, and faster metrology throughput demands.

In this article, we introduce the concept of the near-field metalens into conventional optical scatterometry and through-focus optical microscopy to meet two specific challenges in OCD metrology:

- 1) ultra-narrow focusing of the beam to do metrology using a $1 \mu\text{m} \times 1 \mu\text{m}$ scatterometry target, and
- 2) enhancing the signal associated with the 7 nm node patterned wafer.

ULTRA-SMALL TARGET DESIGN

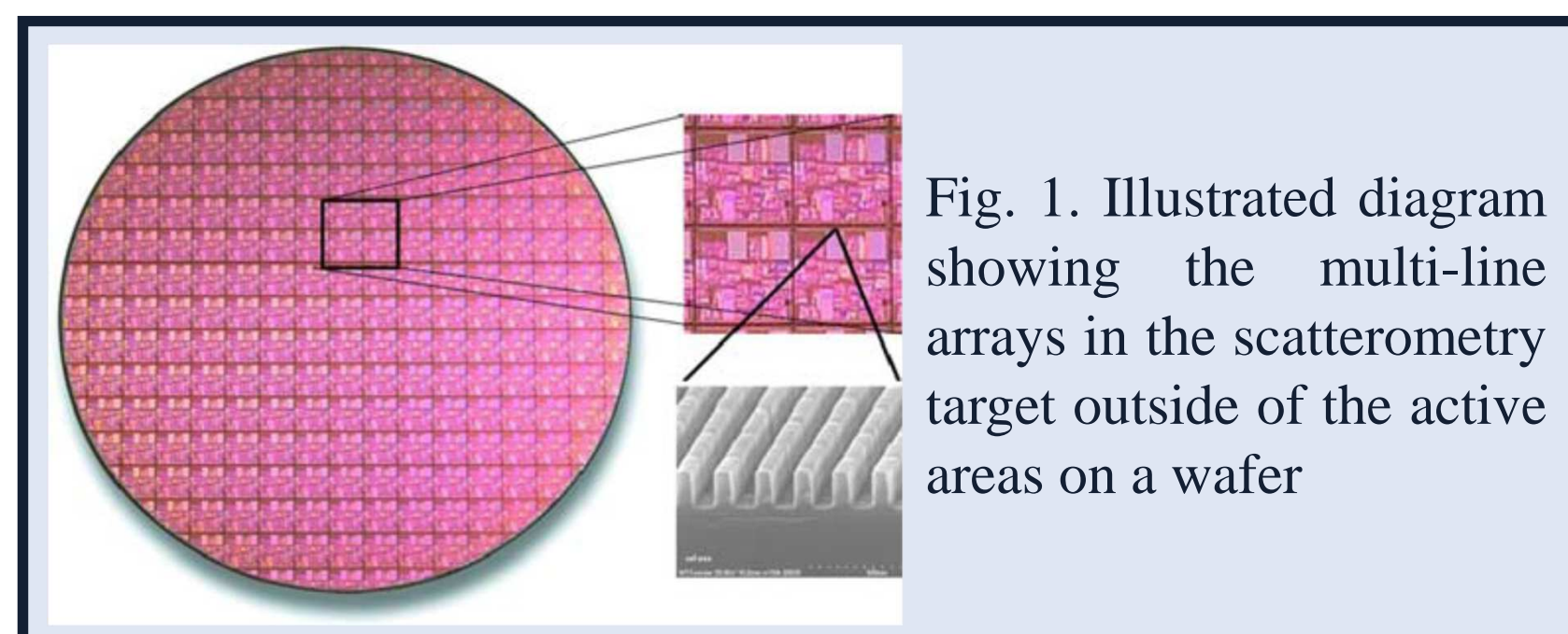


Fig. 1. Illustrated diagram showing the multi-line arrays in the scatterometry target outside of the active areas on a wafer

Challenges:

- a) Reduced scatterometry target size, with some recent projections of targets as small as $10 \mu\text{m} \times 10 \mu\text{m}$.
- b) Reducing the size of a focused beam spot for a multi-wavelengths source remains as a challenging engineering issue⁴.

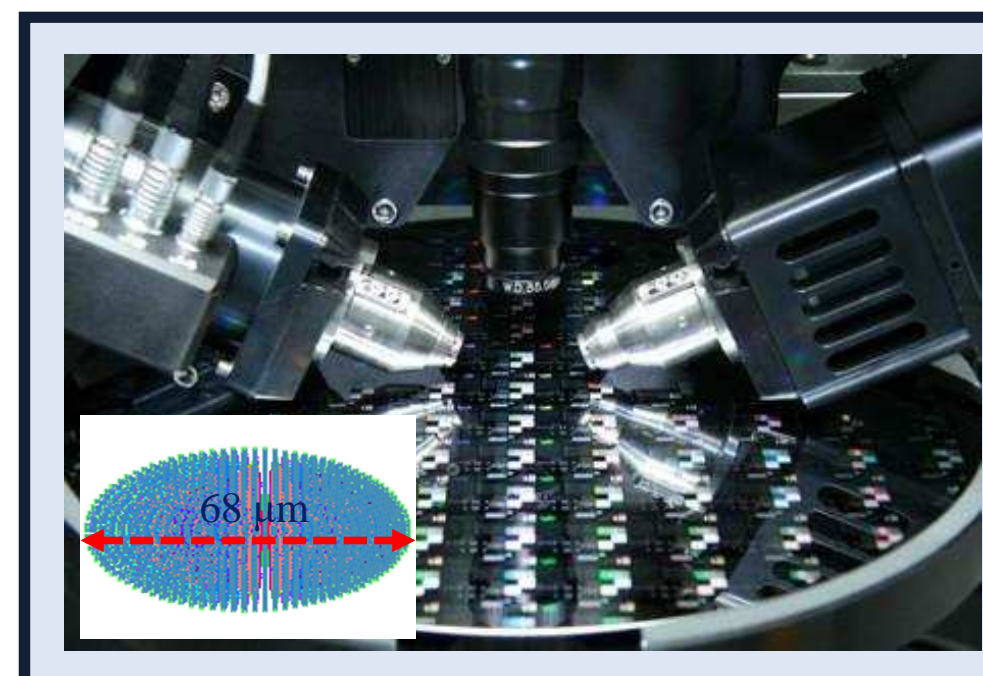


Fig. 2. Typical microspot generation setup in an optical scatterometer for small target metrology. The inset is a simulated focused spot ($68 \mu\text{m}$ long) on the wafer plane.

Goals:

- a) Realizing the metrology of a scatterometry target with a size down to $1 \mu\text{m} \times 1 \mu\text{m}$ and even smaller;
- b) In support of multi-wavelengths source for one-shot measurement;
- c) In support of angle-resolved metrology for decoupling the correlations among fitting parameters

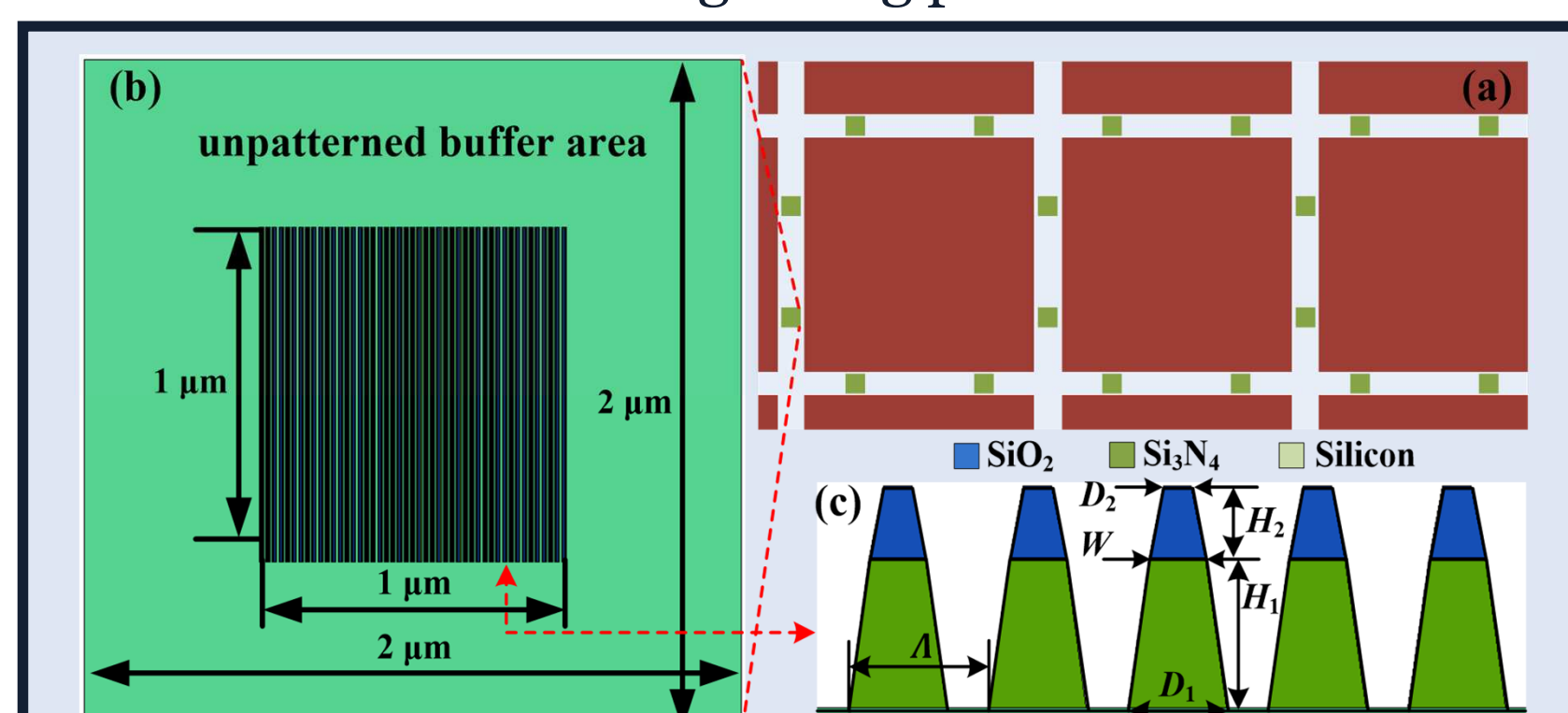


Fig. 3. (a) Schematic (not to scale) of the placement of (CD) scatterometry targets relative to the active area in semiconductor manufacturing. (b) Dimensions of the target and the buffer area. (c) Cross-section geometry of the multi-line array.

DESIGN OF MICROLENS

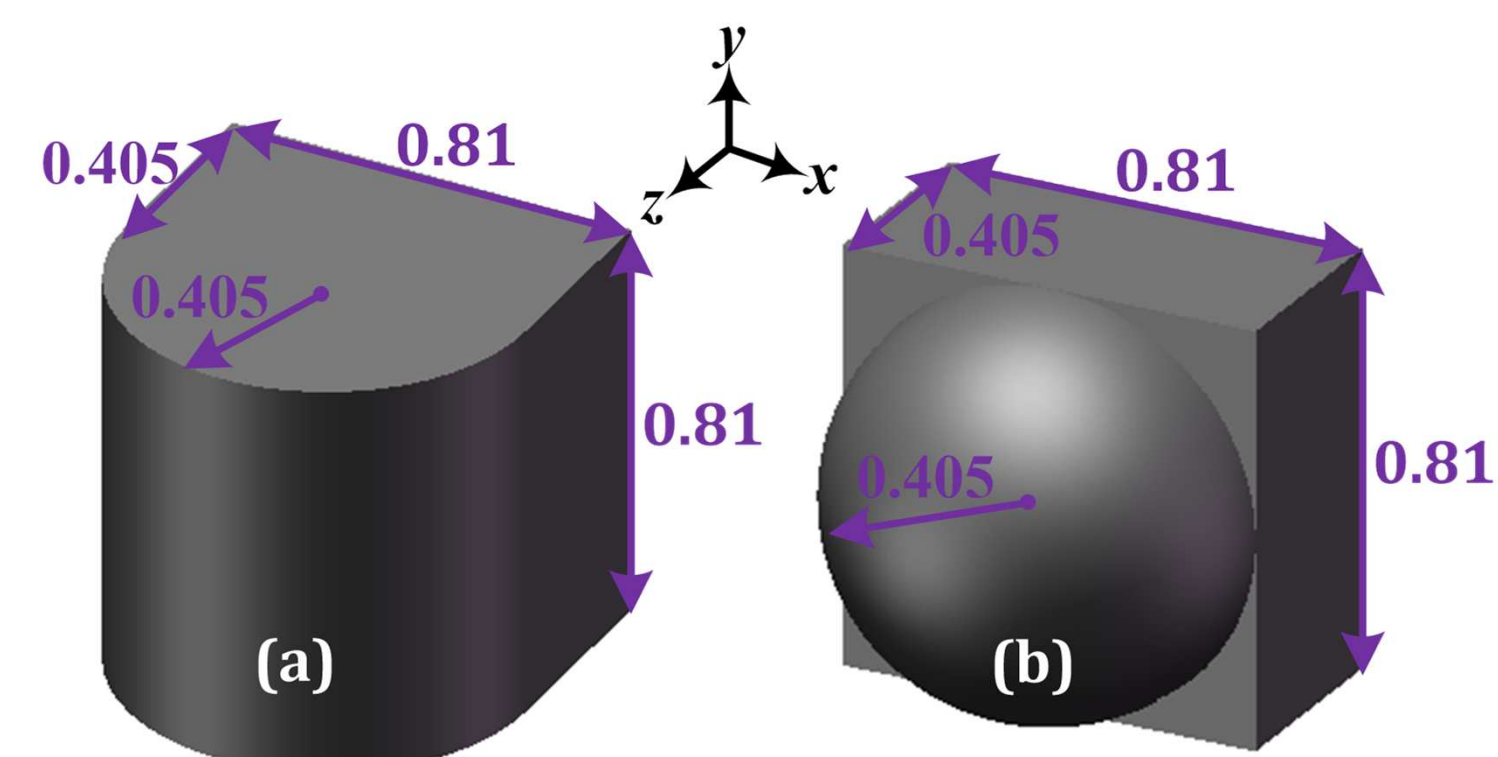


Fig. 4. Microlens with different end structures. The material is SiO_2 and the unit of measurement is μm .

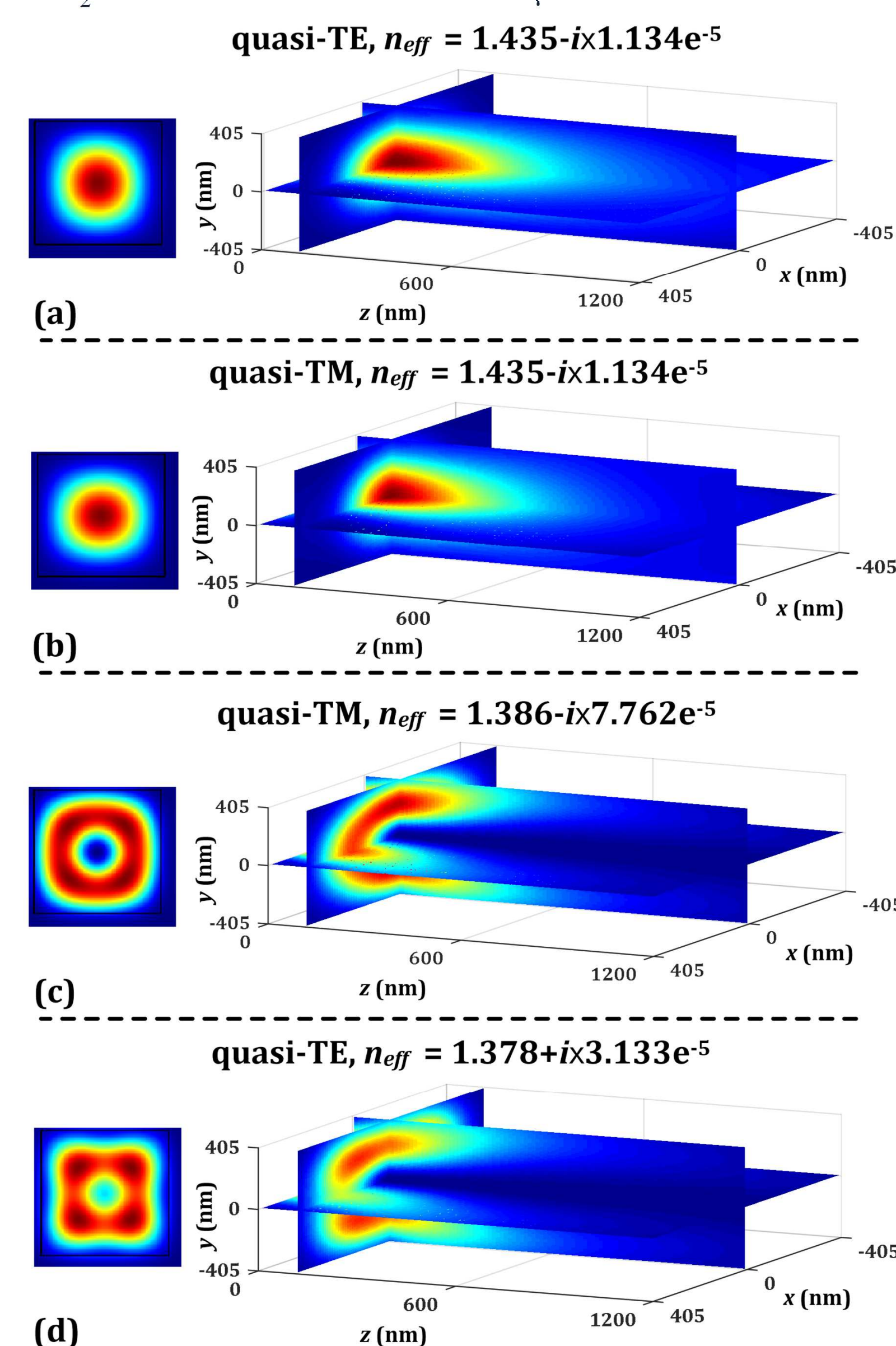


Fig. 5. (left) Eigenmode excitation profile (intensity of electric field) and (right) resulting shadow side field distribution for the half-cylinder asymmetrical microstructure shown in Fig. 4(a). Here, $n_{\text{eff}} = \beta \times \lambda / (2\pi)$, where λ is the free-space wavelength, i.e., 405 nm. Parts of the figures are taken from Ref. 5.

Conclusions:

- a) The fundamental eigenmodes of the SiO_2 supporting stage govern the focusing property of the microlens.
- b) The half-cylinder produces a longer beam than the hemisphere, which indicates a wider adjustable range for the incident angle in consideration of collision.
- c) For a fixed geometry, the length of the focused beam on the shadow side of the microlens increases with the decrease of wavelength.

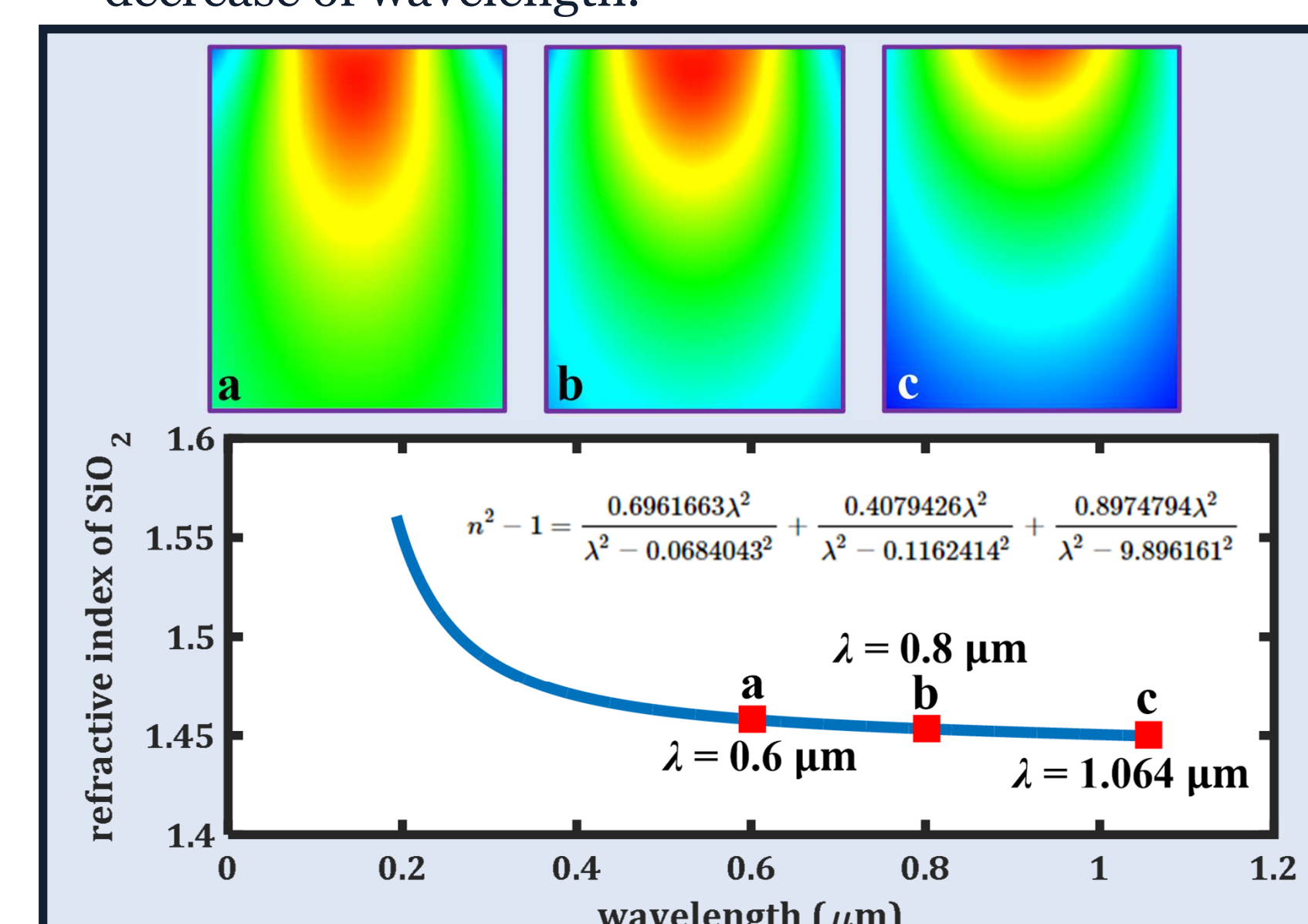


Fig. 6. (bottom) Dispersion of SiO_2 for 210-1064 nm and (top) focused beams generated on the shadow side of the microlens under the activation of the TE01 eigenmode of the supporting stage at the three wavelengths marked by a, b, c, respectively.

BEAM SPOT MODELING

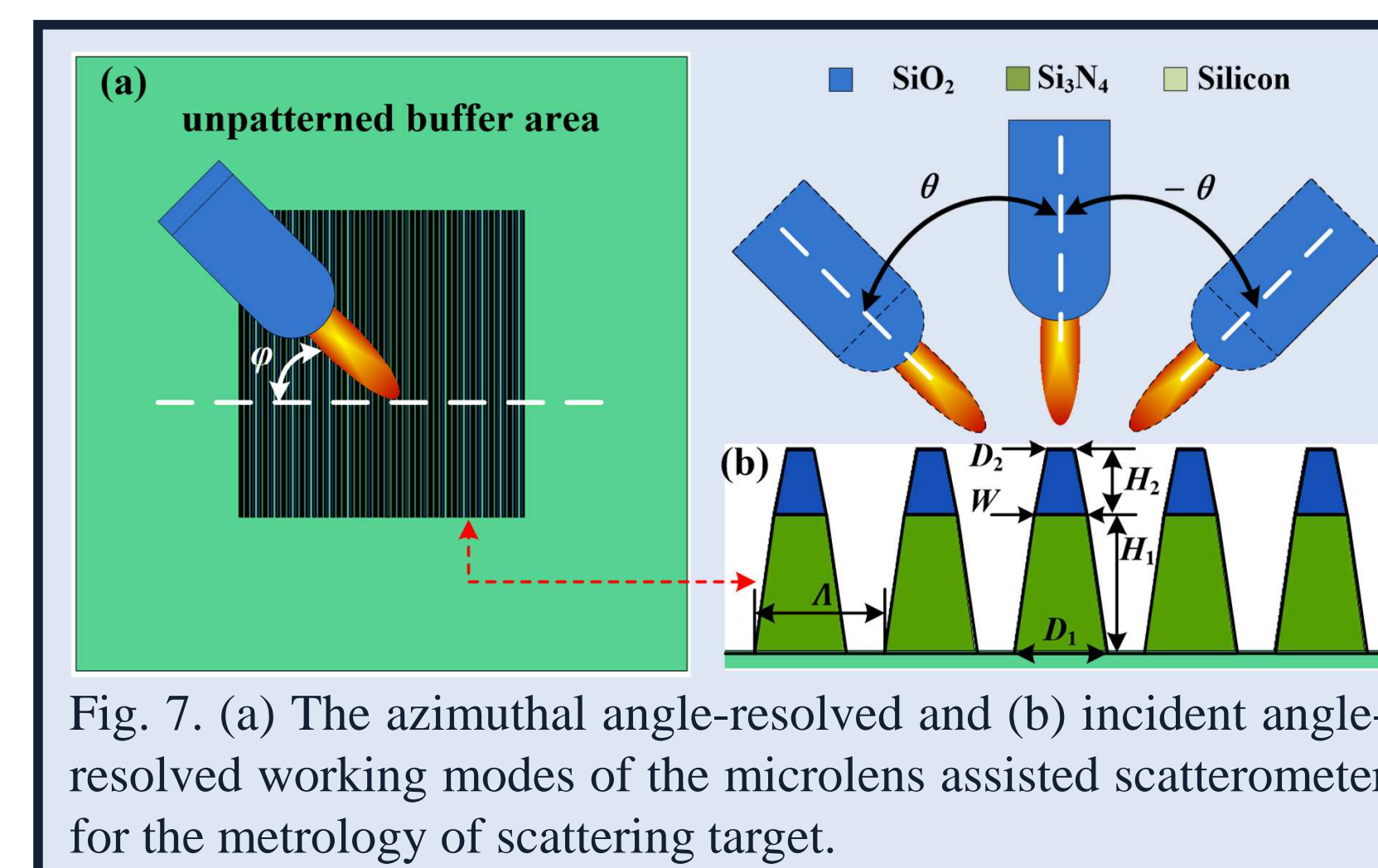


Fig. 7. (a) The azimuthal angle-resolved and (b) incident angle-resolved working modes of the microlens assisted scatterometer for the metrology of scattering target.

Note: Shrinking the working wavelength enables the reduction of the size of the illumination beam spot.

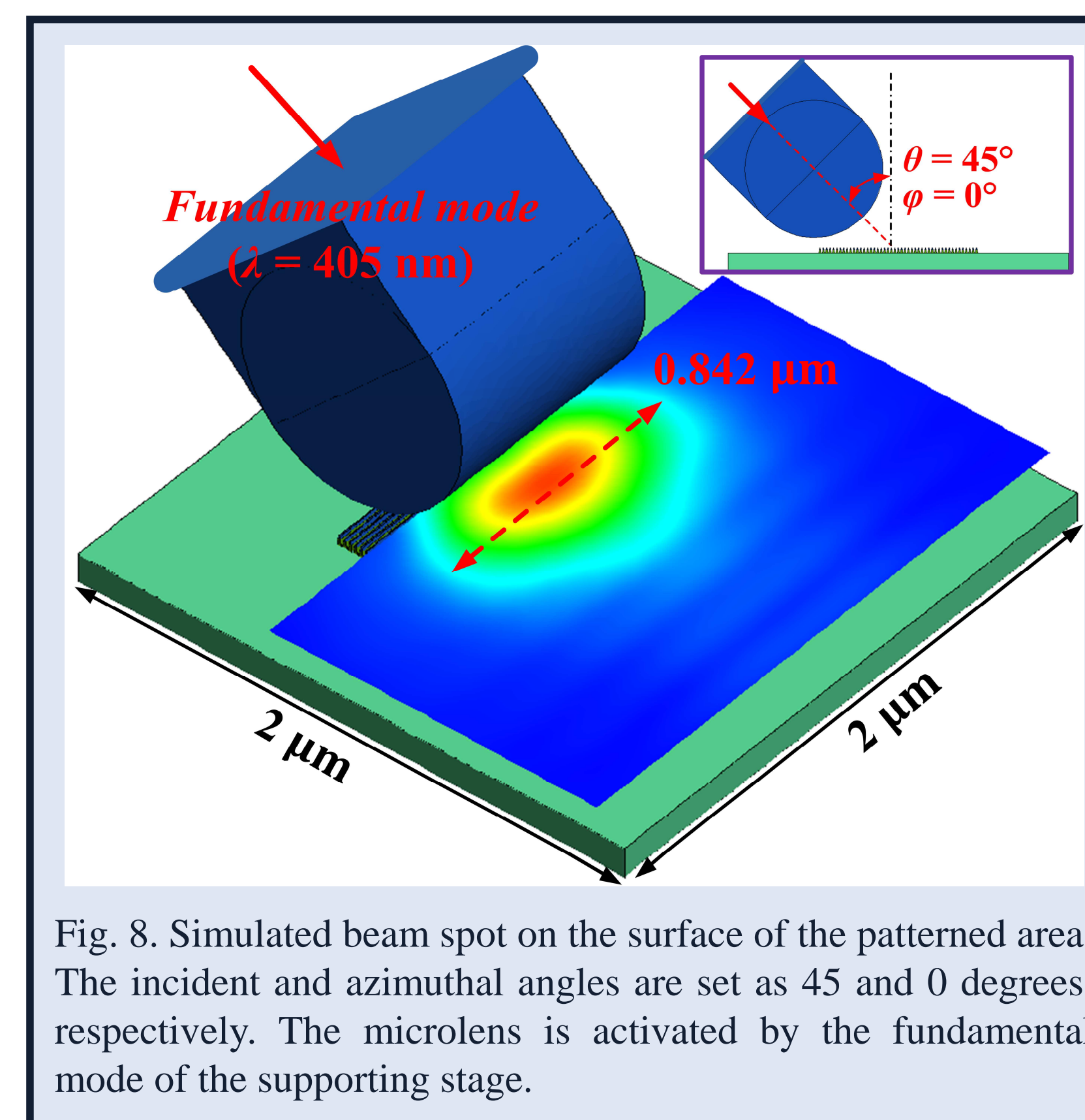


Fig. 8. Simulated beam spot on the surface of the patterned area. The incident and azimuthal angles are set as 45 and 0 degrees, respectively. The microlens is activated by the fundamental mode of the supporting stage.

HIGH NA IMAGING MODELING

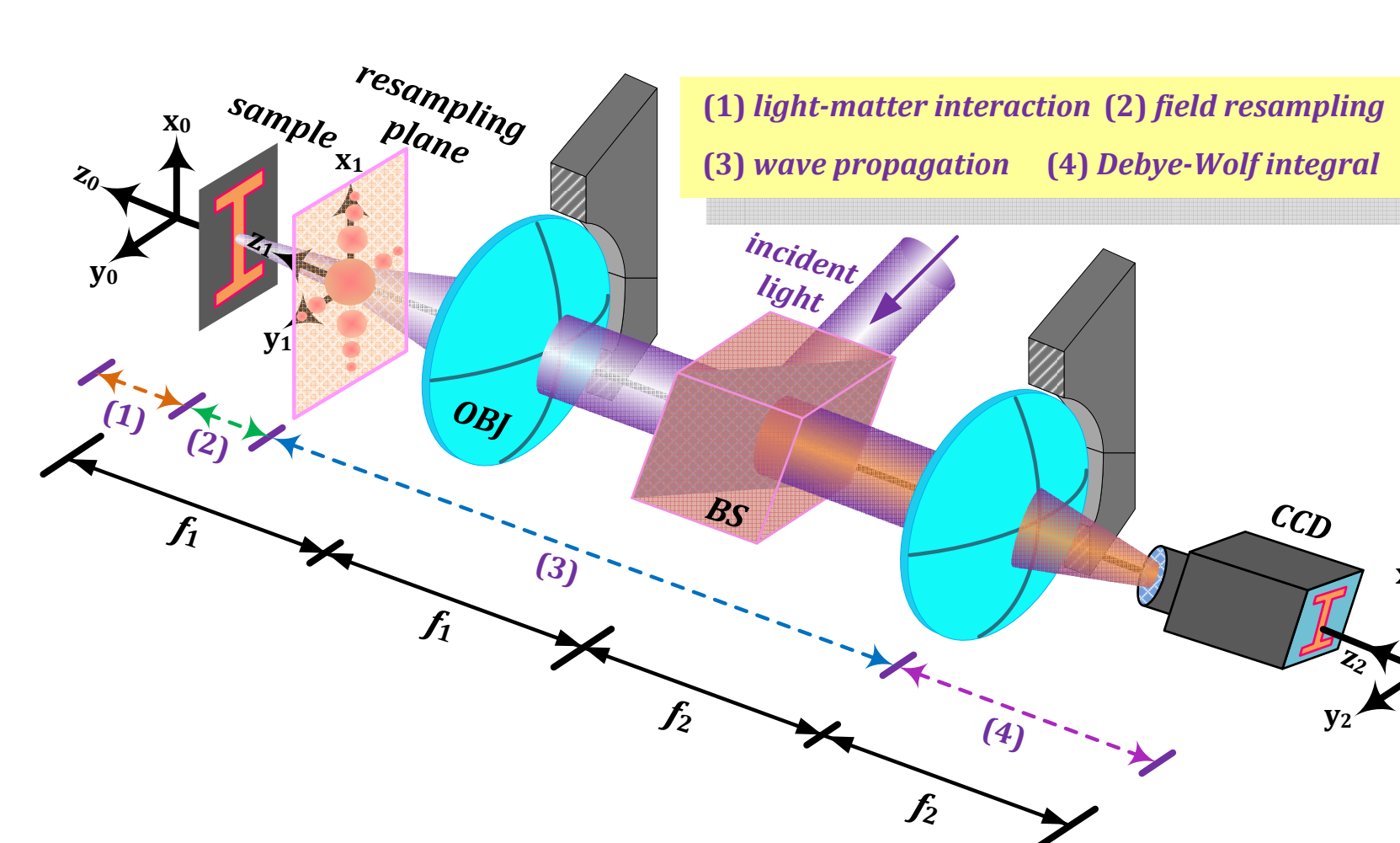


Fig. 9. Diagrammatic description of the systematic simulation model for computing the image of an arbitrary object in epi-illumination coherent optical microscope. OBJ, objective; BS, beam splitter; CCD, charge coupled device. The NA of the objective is set as 0.9 and the magnification factor of the system is fixed at 206.

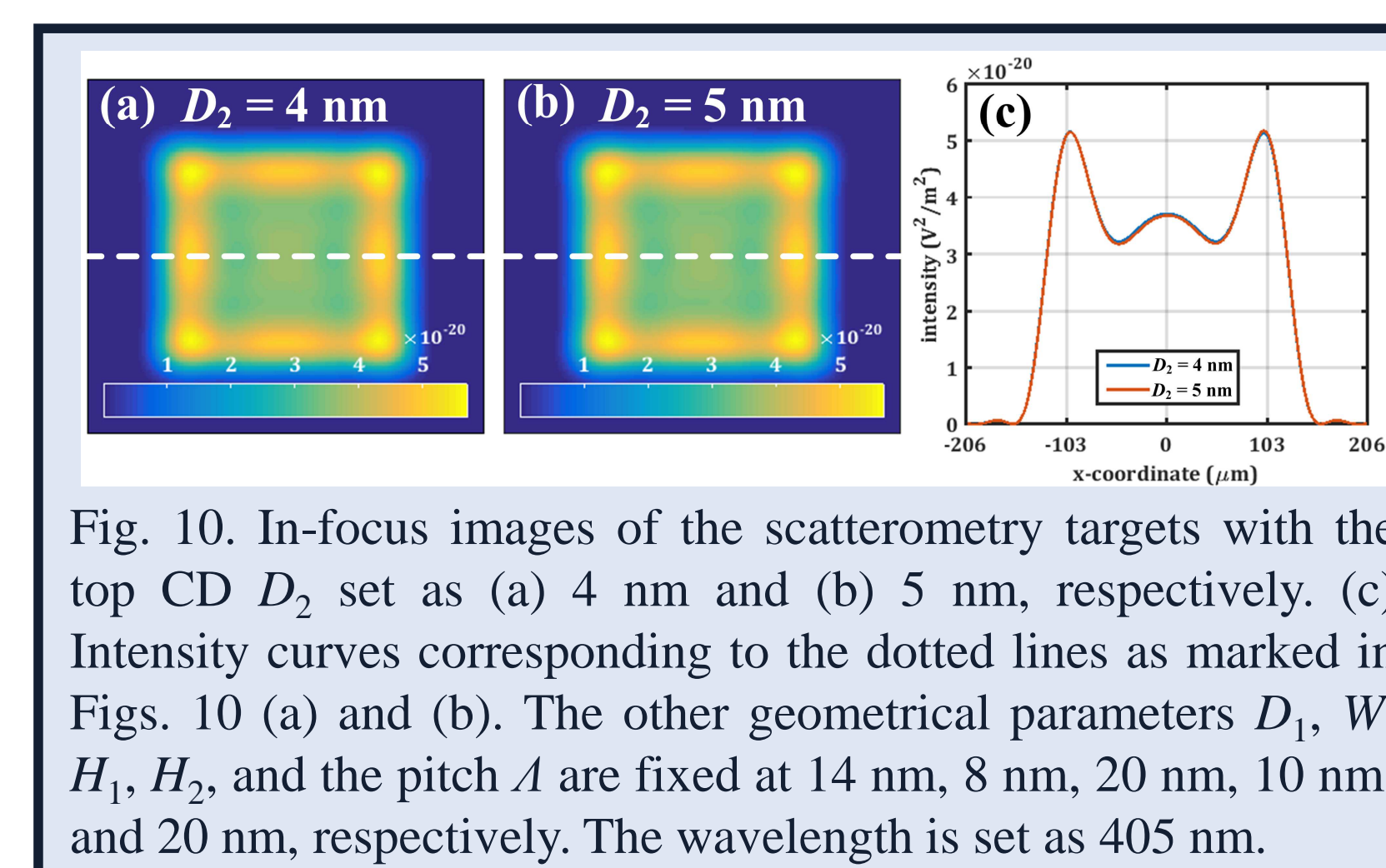


Fig. 10. In-focus images of the scatterometry targets with the top CD D_2 set as (a) 4 nm and (b) 5 nm, respectively. (c) Intensity curves corresponding to the dotted lines as marked in Figs. 10 (a) and (b). The other geometrical parameters D_1 , W , H_1 , H_2 , and the pitch Λ are fixed at 14 nm, 8 nm, 20 nm, 10 nm, and 20 nm, respectively. The wavelength is set as 405 nm.

Conclusions:

For the multi-line array with a top CD (4 nm) that is 100x smaller than the wavelength of the light ($\lambda = 405 \text{ nm}$), 1 nm of bias results in an extremely weak change, which will be easily overwhelmed by the system errors⁶.

ENHANCED THROUGH-FOCUS IMAGES

We propose a near-field metalens based methodology for improving the through-focus differential signal (TFDS) associated with the critical dimension of the 7 nm node (and even below) pattern on the scatterometry target.

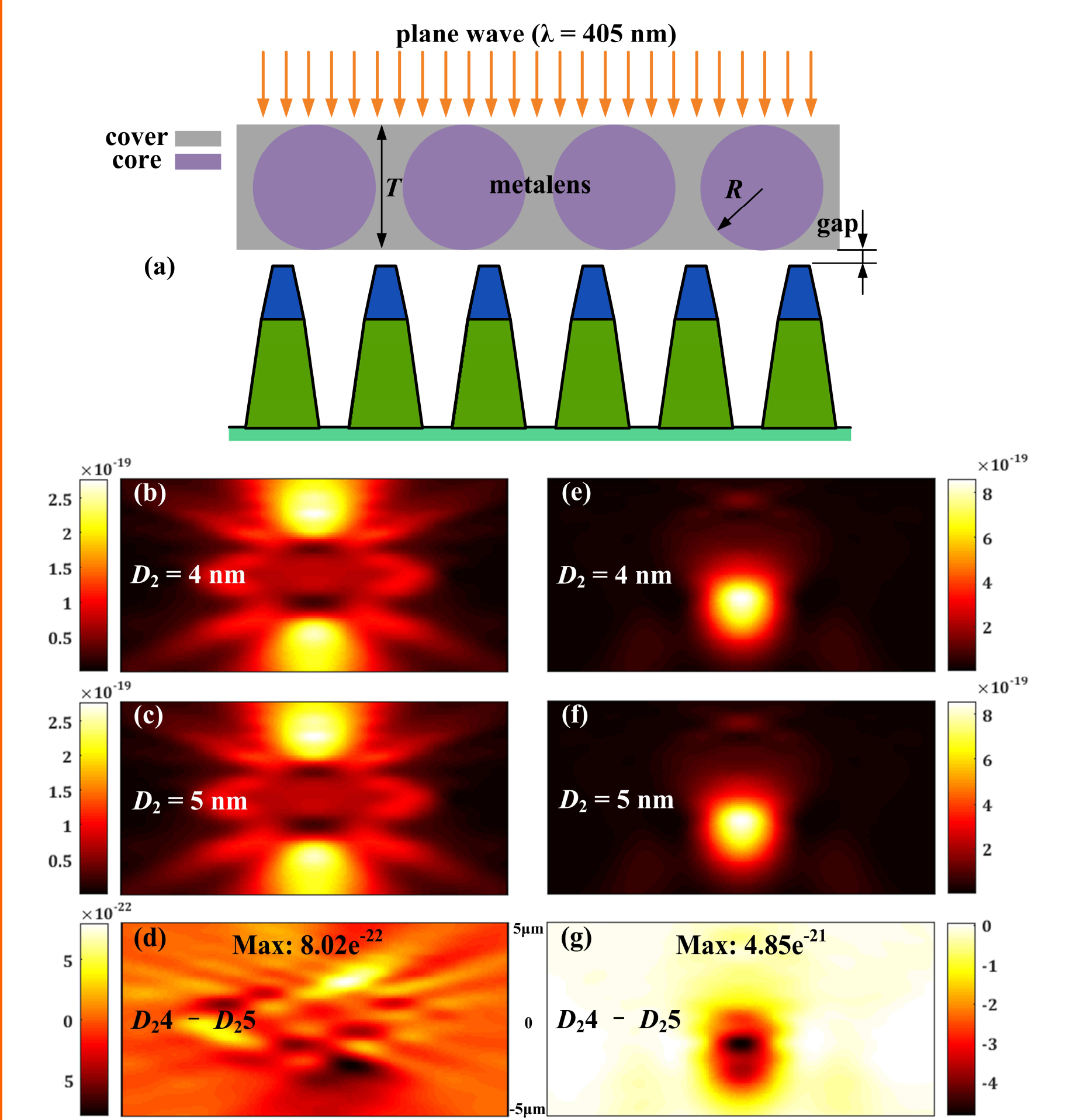


Fig. 11. (a) Measurement setup of the metalens assisted OCD metrology. The materials of the cover layer and the core (microsphere) are air and SiO_2 , respectively. Other parameters, W , H_1 , H_2 , D_1 , Λ , G , R , and T , are fixed at 8 nm, 20 nm, 10 nm, 14 nm, 20 nm, 10 nm, 2430 nm, and 4860 nm, respectively. Simulated through-focus images (TFIs) for the sub-10 nm nanostructure with a top CD (D_2) of (b) 4 nm and (c) 5 nm and (d) TFDS from subtracting Fig. 11(b) from 11(c) for the conventional microscope. (e-g) corresponding figures for the metalens assisted setup. The x and y ranges for Fig. 11(b-g) are shown in Fig. 11(g). Normal incidence with unit amplitude is utilized for all the simulations.

$$\text{Enhancement factor} = \frac{\text{Max}_{\text{metalens}}}{\text{Max}_{\text{conventional}}} = 6.05$$

ACKNOWLEDGMENTS

This work was funded in part by Cisco Systems Inc. (gift award CG 587589). We are grateful to them for access to their Arcetri computing cluster.

REFERENCES

1. C. J. Raymond, M. R. Murnane, S. L. Prins, S. S. H. Naqvi, J. W. Hosch, and J. R. McNeil, "Multiparameter grating metrology using optical scatterometry," *J. Vac. Sci. Technol. B* **15**, 361-368 (1997).
2. J. Zhu, S. Liu, X. Chen, C. Zhang, and H. Jiang, "Robust solution to the inverse problem in optical scatterometry," *Opt. Express* **22**, 22031-22042 (2014).
3. J. Qin, R. M. Silver, B. M. Barnes, H. Zhou, R. G. Dixon, and M. Henn, "Deep subwavelength nanometric image reconstruction using Fourier domain optical normalization," *Light Sci. Appl.* **5**, e16038 (2016).
4. J. Zhu and L. L. Goddard, "Spatial control of photonics nanojets," *Opt. Express* **24**, 30444-30464 (2016).
5. J. Zhu and L. L. Goddard, "Controlling photonics nanojets: from the standpoint of eigenmode," *submitted*.
6. J. Zhu, K. Zhang, N. Davoudzadeh, X. Wang, and L. L. Goddard, "Electromagnetic field modeling for defect detection in 7 nm node patterned wafers," *Proc. SPIE* **9778**, 97780P (2016).